J. Electroanal. Chem., 125 (1981) 41—51
Elsevier Sequoia S.A., Lausanne — Printed in The Netherlands

SENSITIVITY OF AN INTEGRATING DIFFERENTIAL PULSE POLAROGRAPH TO INTERFERING SIGNALS

SAM BEN-YAAKOV * and H. GUTERMAN

Department of Electrical Engineering, Ben-Gurion University of the Negev, Beer-Sheva (Israel)

(Received 29th September 1980; in revised form 27th January 1981)

ABSTRACT

A model for error response in differential pulse anodic stripping voltammetry in the presence of a deterministic signal is proposed and successfully applied to predict the error in a practical instrumentation system.

It is demonstrated that the system is efficient in rejecting 50 Hz and its harmonics, but produces a relatively large error for interfering signals of low frequencies. The sensitivity of the method in the determination of Cd(II) is estimated theoretically and verified experimentally for the polarograph studied.

INTRODUCTION

Electrochemical methods of polarography and voltammetry have great potentiality for the determination of a number of dissolved heavy metals [1—6]. Anodic stripping voltammetry (ASV), which increases sensitivity by preconcentrating the metals on the working electrode, has been shown to be applicable for the analysis of heavy metals in the sub-ppb($\mu g\ l^{-1}$) levels [7—10]. However, the usefulness of the method as an analytical tool for the determination of trace heavy metals depends on many chemical, physical and operational considerations. Among these, the question of sensitivity is central, since the base-line concentration of dissolved trace heavy metals, such as Zn, Cd, Pb and Cu, in natural waters is very low [8].

A number of methods have been proposed to increase the sensitivity of ASV. Improved pulse technique [3,8] and base-line subtraction [9,10] are but two examples of the many approaches that have been examined in an attempt to improve the sensitivity of the ASV technique. However, since the ASV signals, like any signal which represents electrical or physical quantities, are invariably accompanied by noise, the sensitivity of any ASV technique is ultimately limited by the signal-to-noise ratio. The noise sources can be external noise, such as power-line interference, electronic noise or electrochemical noise, generated at the interface [11—13]. Once the nature of the noise and the interfer-

* To whom correspondence should be addressed.

0022-0728/81/0000—0000/$02.50

ing effects are known, one could explore various approaches for signal processing techniques, to improve further the sensitivity of the analytical method.

This paper presents preliminary results of noise analysis in differential pulse voltammetry, which has gained wide acceptance as an analytical tool [8—10]. The investigation was conducted for a given instrument architecture, which is similar to the design of commercial instruments. The response of the system to a deterministic sinusoidal source of fixed amplitude is considered in this work.

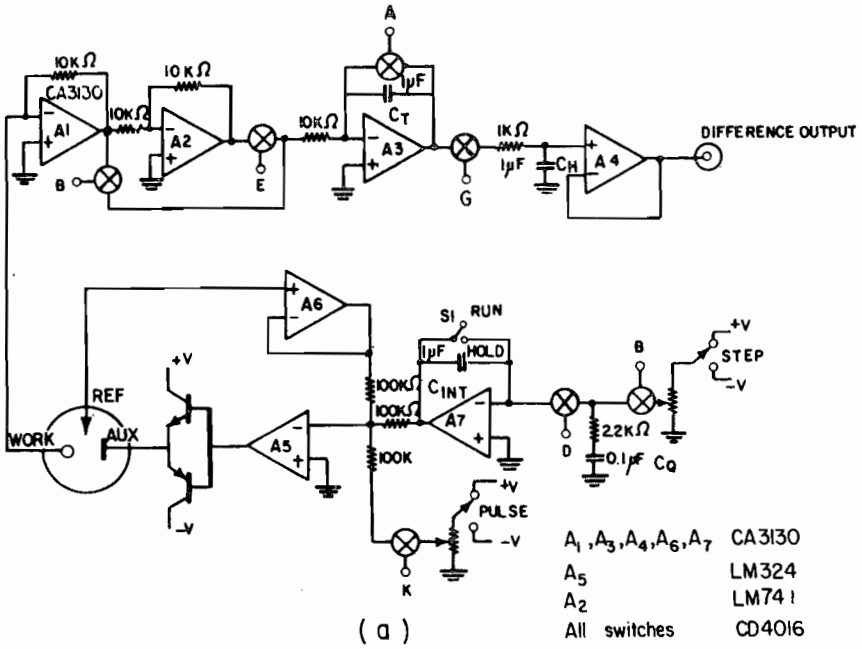

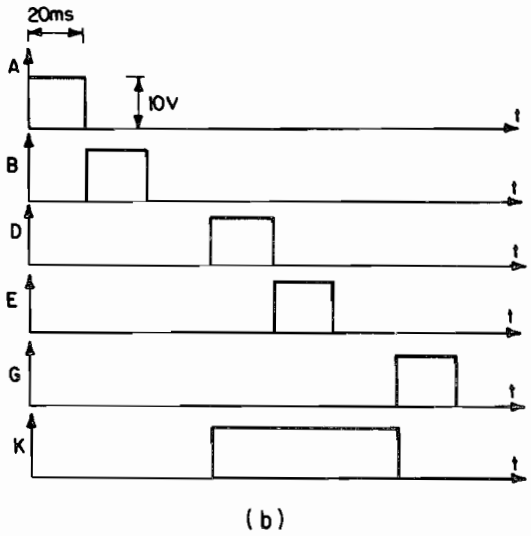

Fig. 1. (a) Schematic diagram of polarograph applied in the present study; (b) associate timing diagram of control pulses.

The results are therefore directly applicable to problems such as power-line interferences and other cases where the characteristics of the interfering signals (internal or external) are known.

SYSTEM CONFIGURATION

The design of the polarographic analyser of this study (Fig. 1a) is similar in concept to the differential polarograph described by Vassos [7], but it uses a pulse excitation superimposed on a staircase rather than a dc ramp. The pulse form (Fig. 2A) is similar to that used in an earlier investigation by one of the authors [10], and described by others [2,3]. The step and pulses are synchronized to the power-line frequency to minimize the interference due to spurious power-line signals (50 Hz in Israel) and harmonics. The operation is controlled by bilateral analog switches which are driven by a logic circuitry, synchronized to the power-line frequency. The timing diagram of the control pulses is given in Fig. 1b.

The system is divided functionally in two parts: the potentiostat and the differential signal processor. Sample and hold technique is used to generate the step to which the pulse is added by controlling an analog gate. A standard feedback configuration is used for realizing the potentiostat.

The pulsed waveform (Fig. 2A) is formed by A7 and associated circuitry (Fig. 1a). The steps are formed by discharging the charge of C_Q into the integrator (A7). The capacitor C_Q is first charged via switch B to the desired level and then discharged via switch D into the integrator. For each charging—discharging cycle the output of the integrator will increase by $V_{STEP}C_Q/C_{INT}$. The pulse is superimposed on the step by turning on the analog switch K for the pulse period (Fig. 1a).

The WE current is integrated for 20 ms by the integrator A3. The switches B and E sample the current at the end of each step and at the middle 20 ms of

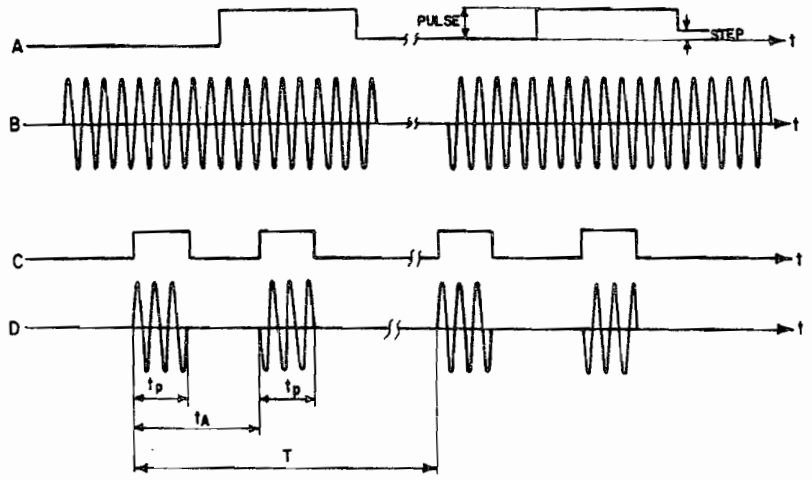

Fig. 2. Timing diagram of polarograph response to a sinusoidal input: (A) potentiostat wave form; (B) interfering signal; (C) sampling and integration periods; (D) sampled interfering signal. In the present study t_p = 20 ms; t_A = 60 ms; T = 1280 ms.

the 60 ms pulse (see timing diagram of Fig. 1b and Fig. 2C). The polarity of the pulse sample is inverted with respect to the base-line sample by means of A2 and the difference is sampled by G and stored on C_H.

MODEL CALCULATIONS

The analysis is performed for a deterministic interfering signal of a sinusoidal waveform and fixed amplitude as depicted in Fig. 2B. The signal is assumed to be present at the input of A1 and also at the output of the potentiostat.

The input signal is sampled twice during each period T (Fig. 2C and 2D). Sampling time is t_p = 20 ms with $t_A = 3t_p$ and $T = 64t_p$ (Fig. 2D). Hence, the integrator's input is a periodic signal that is formed by the pulsed sinusoidal signal (Fig. 2C and D). The integrator's signal can therefore be expressed as

$$F_i(t) = A[u(t)\sin(\omega t + \phi) - u(t - t_p)\sin(\omega t + \phi) - u(t - t_A) \times \sin(\omega t + \phi) + u(t - [t_A + t_p])\sin(\omega t + \phi) + u(t - T)\sin(\omega t + \phi)] \quad (1)$$

where A is the amplitude of the interfering signal and u is the unit step function. Then

$$F_i(t) = A\sin(\psi)[u(t) - u(t - t_p) - u(t - t_A) + u(t - [t_A + t_p]) + u(t - T)] \quad (2)$$

where $\psi = \omega t + \phi$.

The Laplace transform of eqn. (2) is obtained by applying the trigonometric relation:

$$\sin(\omega t + \phi) = \sin(\omega t)\cos(\phi) + \cos(\omega t)\sin(\phi)$$

$$F_i(s) = \frac{A}{s(s^2+1)}[1 - e^{-st_p} - e^{-st_A} + e^{-s[t_A+t_p]} + e^{-sT}][\cos(\phi) + s\sin(\phi)] \quad (3)$$

The transfer function of the integrator is

$$H(s) = s_1/s; \qquad s_1 = 1/RC \quad (4)$$

Using eqns. (3) and (4) the output of the integrator is expressed as

$$F_o(s) = H(s)F_i(s)$$

$$= \frac{B}{s^2}[1 - e^{-st_p} + e^{-s[t_A+t_p]} + e^{-sT}]\left[\frac{\cos(\phi)}{s^2+1} + \frac{s\sin(\phi)}{s^2+1}\right] \quad (5)$$

where $B = As_1$.

The inverse Laplace transform of eqn. (5), from t_i to $t_3 = 4t_p$ is

$$F_o(t)|_{t_1}^{t_3} = (2B/\omega)\cos(\phi)\,[\cos(\omega t_3) + \cos(\omega t_i) + \cos(\omega t_p) - \cos(\omega t_A)]$$

$$+ \sin\phi[-\sin(\omega t_3) + \sin(\omega t_A) + \sin(\omega t_p) - \sin(\omega t_i)] \quad (6)$$

which can be written for any given frequency as

$$F_o(t)|_{t_1}^{t_3} = D\cos(\phi) + E\sin(\phi) \quad (7)$$

This equation relates the output signal $F_o(t)$ to the phase angle of the interfering signal at the integration period. The error will be constant (dc) if ϕ is constant. This could be achieved by synchronizing the sampling period to the interfering signal. In the general case, however, ϕ will not stay constant resulting in a time-dependent $F_o(t)$. The maximum and minimum of the output signal function $F_o(t)$ (eqn. 7) is derived by differentiating eqn. (7) with respect to ϕ and equating the derivative to zero:

$$\partial F_o/\partial\phi = -D\sin(\phi) + E\cos(\phi) \tag{8}$$

From which:

$$E/D = \sin(\phi)/\cos(\phi) = \tan(\phi) \tag{9}$$

It is observed that extreme points are obtained for two possible values of ϕ, ϕ_1 and ϕ_2 which are related by:

$$\phi_1 = \phi_2 + 180^\circ \tag{10}$$

The maximum and minimum are identified by the second derivative:

$$\partial^2 F_o/\partial\phi^2 = -D\cos(\phi) - E\sin(\phi) \tag{11}$$

Hence:

$$F_o = -\partial^2 F_o/\partial\phi^2 \tag{12}$$

Applying eqns. (9) and (12) one obtains:

$$F_o(t)|_{t_i}^{t_3} = E\left[\frac{\cos(\phi_1)}{\tan(\phi_1)} + \sin(\phi_1)\right] = E\left[\frac{\cos(\phi_1)^2 + \sin(\phi_1)^2}{\sin(\phi_1)}\right] = \frac{E}{\sin(\phi_1)} \tag{13}$$

$$E = D\tan(\phi_1)$$

But since

$$\sin(\phi_1) = \tan(\phi_1)/\pm\sqrt{1 + \tan^2(\phi_1)}$$

$$F_o(t)|_{t_i}^{t_3} = \pm\sqrt{D^2 + E^2} \tag{13A}$$

The maximum and minimum of output signal are then:

$$F_o(t)|_{t_i}^{t_3}\,\max = \sqrt{D^2 + E^2} \tag{14}$$

$$F_o(t)|_{t_i}^{t_3}\,\min = -\sqrt{D^2 + E^2} \tag{15}$$

In the second stage of the analysis the interfering signal is assumed to be present at the output of the potentiostat and fed to the amplifier via a dummy cell represented by an equivalent R_c and C_c (Fig. 3). The modified function is derived by applying the transform functions

$$R(S) = R_cC_c/(sR_cC_c + 1) \tag{16}$$

From which:

$$|R| = \frac{\omega C_c R_F}{\sqrt{\omega^2 C_c^2 R_c^2 + 1}} A' \tag{17}$$

where A' is the amplitude of the input signal to the dummy cell. Applying the

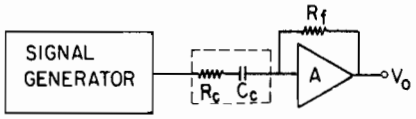

Fig. 3. Schematic diagram of experimental set-up for measuring the response of the polarograph and dummy cell to an interfering signal.

analysis detailed above:

$$F_o(t)|_{t_i}^{t_3} \max = \left|\frac{K}{\sin(\phi_1)}\right| \tag{18}$$

$$F_o(t)_{t_i}^{t_3} \max = +\sqrt{K^2 + M^2} \tag{18A}$$

$$F_o(t)|_{t_i}^{t_3} \min = -\left|\frac{K}{\sin(\phi_1)}\right| \tag{19}$$

$$F_o(t)|_{t_i}^{t_3} \min = -\sqrt{K^2 + M^2} \tag{19A}$$

where

$$K = \frac{2|R|s_1}{\omega}(\cos(\omega t_3) + \cos(\omega t_i) - \cos(\omega t_p) - \cos(\omega t_A))$$

$$M = \frac{2|R|s_1}{\omega}(-\sin(\omega t_3) + \sin(\omega t_A) + \sin(\omega t_p) - \sin(\omega t_i))$$

The relative output error is then defined as the ratio of the maximum deviation to the input amplitude A'.

$$E_r \triangleq |F_o(t)|_{t_i}^{t_3} \max - F_o(t)|_{t_i}^{t_3} \min| / A'$$

$$= \frac{2F_o(t)|_{t_i}^{t_3} \max}{A'}$$

$$= \frac{2F_o(t)|_{t_i}^{t_3} \min}{A'} \tag{20}$$

The total noise power E_n, for a given bandwidth Δf is then given by

$$E_n^2 \triangleq \int_{\Delta f} [A'(f)E_r]^2 \, df \tag{21}$$

EXPERIMENTAL

Instrumentation

Measurements were made with a Ben-Gurion University (B.G.U.) Model E.I. 204 polarographic analyzer and recorded with a storage oscilloscope, Textronix Model 5113, with dual time base (5B12N) and a four-channel amplifier (5A14N) plug-ins.

The input signal source was a Wavetek Model 164 function generator. The noise was measured with an autoranging R.M.S. voltmeter, Bruel & Kjaer, Type 2426, and a Krohn-Hite filter, Model 3550.

Electrodes and cell

Measurements were carried out in a 50 ml Universal Titration Vessel (Metrohm EA 876-50), with a plastic cover through which the electrodes and the tube carrying the oxygen purging gas (CO_2) were inserted. The solution was stirred with a Teflon-coated stirring bar. A Metrohm Type EA437 silver chloride electrode served as a reference electrode, and a coiled platinum wire was used as an auxiliary electrode.

The working electrode was a thin mercury film electrode (TMFE) deposited on glassy carbon (GC) 3 mm in diameter (Ringesdorf Werke S-10). The electrode face was polished with Hyprez Diamond Compound of 6, 1, and 0.1 μm grade on a Hyprocell Pellon Cloth (Engis Ltd.). The surface finish was checked for scratches with a reflected light microscope.

Reagents and solutions

The test solution was Dahav (Gulf of Eilat, Red Sea), seawater. The plating solution was approximately 2×10^{-5} *M* mercuric nitrate prepared by dissolving the salt (Baker Analyzed Reagent) in seawater. A commercial CO_2 gas, treated with vanadous chloride solution, was used to purge the sample.

Procedure

(A) Calibration curve

The plastic cover, through which the electrodes were inserted was transferred to a 50 ml Universal Titration Vessel containing the Hg plating solution and a −1400 mV potential was applied to the working electrode (WE) for 20 min. Following the plating time, the potential was changed to −200 mV for another 3 min to strip any trace metal deposited during plating. The electrodes were then cleaned with distilled water and placed in the test solution (stored seawater). The solution was deaerated for 10 min, after which the ASV cycle was commenced. The analysis consisted of four steps:

(1) Application of −1000 mV to the WE in a stirred solution with application of CO_2 for 2 min.

(2) Rest period of 30 s for the WE in unstirred solution and no CO_2 stripping at a potential of −1000 mV.

(3) Scanning from −1000 mV to −500 mV (E pulse = 50 mV, E_{step} = 10 mV, T = 1280 ms) and recording the WE current.

(4) Stripping the WE for 30 s at −500 mV in a stirred solution with application of CO_2.

(B) Error response of differential signal processor

The response was obtained by feeding a sinusoidal signal via a 1 kΩ resistor to A1 (Fig. 1a) and recording the output on a storage oscilloscope. Measure-

ment time for each frequency was 5 min, after which the span between the maximum and minimum values were read off the oscilloscope screen.

(C) Error response for the system

The auxiliary electrode and the reference electrode leads were tied together and a dummy cell was connected between this junction and the input of the WE (amplifier A1, Fig. 1). A sinusoidal signal was fed via a 100 kΩ resistor to A5 (Fig. 1). The procedure for determining the noise level at the output followed that outlined above. Dummy cell components were R_c = 63 Ω and C_c = 11.4 μF. These values were found to simulate the response of the cell used.

(D) Transfer response of the dummy cell and amplifier

A sinusoidal signal was fed to the dummy cell (Fig. 3), and the output signal of the WE amplifier (A1, Fig. 1a), was measured with a voltmeter over the desired frequency range. The transfer function (V_{output}/V_{input}) was then measured as a function of frequency.

(E) Measurement of the potentiostat noise

This measurement was made with the cell (see A above). The potential was set to −700 mV and the pulse and step amplitudes were set to zero. The spectral noise power density of the potentiostat was measured with the rms voltmeter and a bandpass filter.

(F) Computation

Model calculations were carried out by a program written in BASIC which was run on a CBM Microprocessor (Commodore Business Machines), and later by a program written in FORTRAN IV which was run on a CYBER 170 computer.

RESULTS AND DISCUSSION

The response of the differential signal processor to an interfering noise of fixed amplitude (Fig. 4) is clearly frequency-dependent. This behavior stems from the integration operation which extends over 20 ms, one cycle of the mains frequency (50 Hz in Israel). Complete rejection is obtained at 50 Hz and harmonics, whereas partial rejection is obtained at

$(17 + m50)$Hz; $\quad m = 0, 1, 2, \ldots, \infty$

$(33 + m50)$Hz; $\quad m = 0, 1, 2, \ldots, \infty$

Minimum rejection, i.e. maximum interference, is obtained for:

$(10 + m50)$Hz; $\quad m = 0, 1, 2, \ldots, \infty$

$(25 + m50)$Hz; $\quad m = 0, 1, 2, \ldots, \infty$

$(40 + m50)$Hz; $\quad m = 0, 1, 2, \ldots, \infty$

It should be emphasized, though, that the response of Fig. 4 is the worst case (largest interference) for each frequency, as calculated from eqn. (20). The

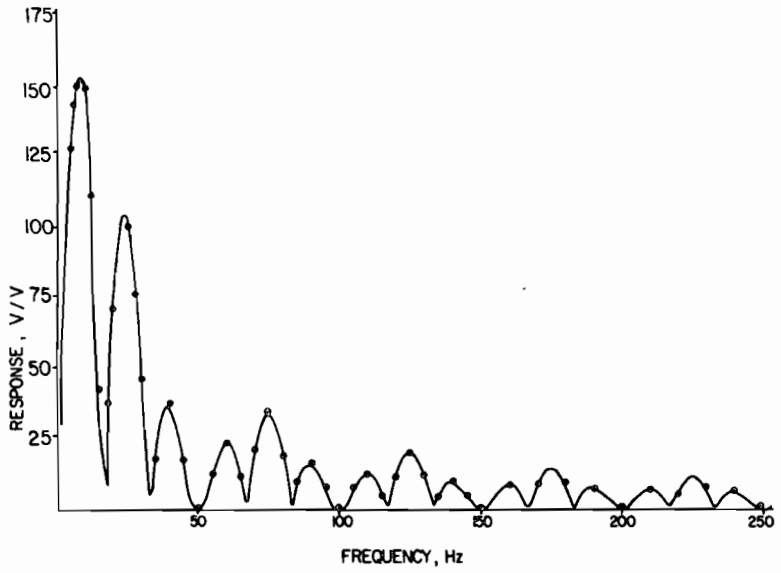

Fig. 4. The response of the differential processor to an interfering signal fed at the input to A1 (Fig. 1). (————) Calculated values; (⊙) measured values; interfering noise: 20 mV pp.

response at each frequency is a function of the phase angle of the interfering signal with respect to the sampling periods (eqns. 1 and 2). The model calculation and experimental determination were carried out for the largest interference at each frequency.

The response of Fig. 4 represents the sensitivity of the system to an interfering signal which is injected (or generated) at the input of the WE amplifier, A1.

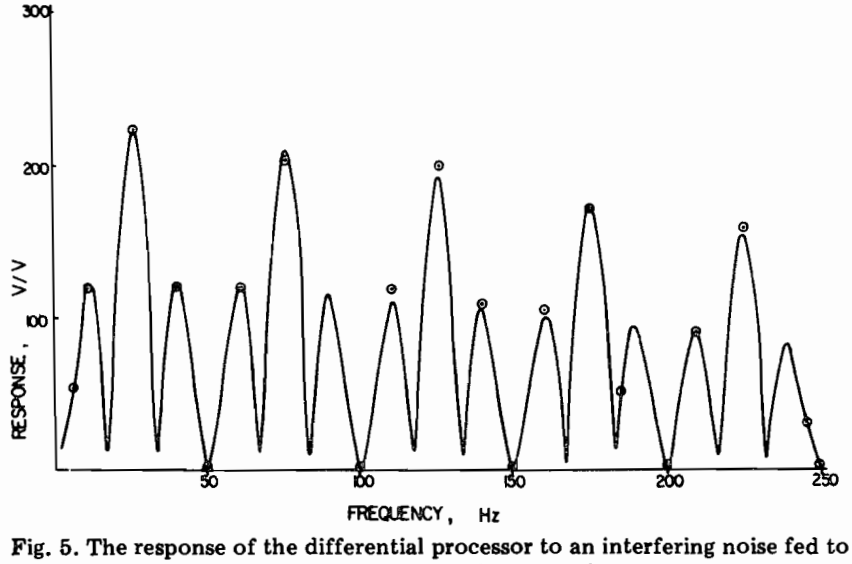

Fig. 5. The response of the differential processor to an interfering noise fed to the dummy cell (Fig. 3). (————) Calculated value; (⊙) measured values.

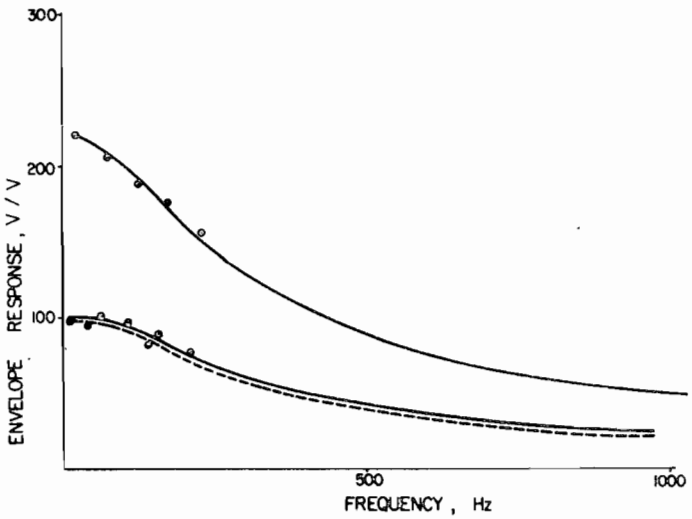

Fig. 6. Peaks envelope of the response of Fig. 5 extended to 1000 Hz. Interfering noise: 1 mV pp. The broken line in the envelope of the smallest peaks of Fig. 5. (———, - - - - -) calculated values; (⊙) measured values. Interfering noise: 1 mV pp.

However, an extra transfer function (eqn. 17), must be taken into account when the interfering signal is present at the output of the potentiostat. The cell represents a high-pass network (eqn. 17) which attenuates the low frequencies, as compared to frequencies above the pole frequency (218 Hz in the present case). Hence, the overall response (Fig. 5) to an interfering signal is more regularly spaced along the frequency spectrum. The envelopes of the peaks (Fig. 6) show a relatively fast decrease up to 250 Hz and then a much slower change with frequency. The total noise expected at the output will depend on the spectrum of the interfering signal and its effective bandwidth. The response to an interfering noise could be calculated by eqn. (21):

$$E_n^2 = \int_0^{f_{max}} [E_r^2 \, \bar{e}_n^2(f)] \, df \tag{22}$$

where f_{max} is the highest frequency of interest and $\bar{e}^2(f)$ is the noise power density.

As an example of practical noise analysis we consider here the performance of the polarograph used in the present study.

The noise sensitivity of the polarograph is limited by the element with the narrowest bandwidth. In the present case, A1 (Fig. 1) with a bandwidth of approximately 2 kHz (when the present dummy cell is used) is limiting the noise spectrum to about 2 kHz. Measurements made at the output of the potentiostat (at the output of A6 of Fig. 1) reveal that the total noise is 0.12 mV over the bandwidth of interest. The contribution of the internal noise of A1 is negligible since the noise density is specified to be 51.4×10^{-9} V/$\sqrt{\text{Hz}}$ [15,16]. The total amplifier noise is thus only 2.3 μV over the 2 kHz bandwidth. The relative noise contribution of other electronic components such as

the amplifiers A_2—A_4 and the analog switches (CMOS) is also negligible since they are added to a relatively high-level signal. Applying eqn. (22) we calculate the expected noise at the processed output of the polarograph to be 0.6 mV. This calculated value agrees well with the independently measured value. This noise level corresponds to an equivalent input noise current (i.e. when referred to the input) of 0.025 μA.

Using the analytical method outlined above and applying the standard addition technique, we have generated a Cd(II) calibration curve for the present instrumentation system. The calibration curve was similar to the one presented earlier [10] in which a similar instrumentation system was used. The slope of the calibration was found to be 0.26 μA/ppb. Hence, the internal noise level of the present instrument correspond to a Cd(II) concentration of 0.096 ppb.

Model calculations suggest that an increase of the integration time by a factor of 2—3 will not change the noise significantly. Hence, signal-to-noise ratio can be improved when using larger integration times, especially if the integration interval is close to the onset of the pulse as pointed out by Valenta et al. [8]. The preceding analysis suggests that the limiting factor of the present polarograph is mainly controlled by the potentiostat noise. Higher instrument sensitivities could be conceivably be obtained by lowering the potentiostat noise. However, this general conclusion pertains to the electronics only and does not take into consideration problems invoked by the electrochemical cell. Background current and interface noise [10—14] will eventually set the sensitivity threshold of the overall system.

REFERENCES

1 H. Siegerman and Q. O'Dom, Am. Lab., 4 (1972) 59.
2 J.H. Christie and R.A. Osteryoung, Anal. Chem., 48 (1976) 869.
3 J.H. Christie, J.A. Turner and R.A. Osteryoung, Anal. Chem., 49 (1977) 1899.
4 U. Eisner, J.A. Turner and R.A. Osteryoung, Anal. Chem., 48 (1976) 1608.
5 J.A. Turner, J.H. Christie, M. Vukovic and R.A. Osteryoung, Anal. Chem., 49 (1977) 1904.
6 S.C. Rifkin and D.H. Evans, Anal. Chem., 48 (1976) 1616.
7 B.A. Vassos, Anal. Chem., 45 (1973) 1292.
8 P. Valenta, L. Mart and H. Rutzel, J. Electroanal. Chem., 82 (1977) 289.
9 H.W. Nurnberg and P. Valenta, in E.D. Goldberg (Ed.), The Nature of the Seawater, Dahlem Konferenzen, Berlin, 1975, p. 87.
10 B. Lazar and S. Ben-Yaakov, J. Electroanal. Chem., 108 (1980) 143.
11 G. Blanc, I. Epelboin, C. Gabrielli and M. Keddam, J. Electroanal. Chem., 62 (1975) 59.
12 G. Blanc, I. Epelboin, C. Gabrielli and M. Keddam, J. Electroanal. Chem., 75 (1977) 97.
13 I. Epelboin, C. Gabrielli, M. Keddam and L. Raillow, J. Electroanal. Chem., 93 (1978) 155.
14 D.Y. Sawyer and J.L. Roberts, Jr., Experimental Electrochemistry for Chemists, Wiley, New York, 1974.
15 R.C.A., Integrated Circuits, R.C.A., 1976.
16 J.Q. Graeme, Q.E. Tobey and L.P. Huelsman (Eds.), Operational Amplifier: Design and Applications, McGraw-Hill, New York, 1971.